Eur. Phys. J. Special Topics **199**, 139–148 (2011)
© EDP Sciences, Springer-Verlag 2011
DOI: 10.1140/epjst/e2011-01509-9

THE EUROPEAN PHYSICAL JOURNAL SPECIAL TOPICS

Regular Article

Kinetics of colloidal fractal aggregation by differential dynamic microscopy

F. Ferri[1], A. D'Angelo[1], M. Lee[2], A. Lotti[1,3], M.C. Pigazzini[1], K. Singh[4], and R. Cerbino[5,a]

[1] Dipartimento di Fisica e Matematica, Università degli Studi dell'Insubria, via Valleggio 11, 22100 Como, Italy
[2] School of Physics and Astronomy, University of Glasgow, Glasgow, G12 8QQ, UK
[3] Centre de Physique Théorique, École Polytechnique, Centre National de la Recherche Scientifique, 91128 Palaiseau, France
[4] Institut National de la Recherche Scientifique-Énergie, Matériaux et Télécommunications, 1650, boulevard Lionel-Boulet EMT, Varennes, QC, J3X 1S2, Canada
[5] Dipartimento di Chimica, Biochimica e Biotecnologie per la Medicina, Università degli Studi di Milano, via F.lli Cervi 93, 20090 Segrate, Italy

Received 29 August 2011 / Received in final form 4 October 2011
Published online 7 December 2011

Abstract. We study the kinetics of an aggregation process induced by adding salt to a stable colloidal suspension of 73 nm (diameter) particles. Despite the subdiffraction size of the colloidal particles, the process is monitored via optical microscopy, which is used here to obtain time-resolved scattering information about the colloidal aggregates. The radius of the aggregates is determined as a function of time and their fractal dimension is extracted. Our results are compatible with a diffusion limited aggregation process, as independently confirmed by spectral turbidimetry measurements on the same sample.

1 Introduction

The assembly of small colloidal particles into disordered fractal aggregates is an important phenomenon both for fundamental science and for technological applications [1,2]. It is therefore not surprising that a fervent experimental and theoretical activity has been devoted in the past 30 years to unveil the profound concepts associated with colloidal aggregation. A first reason is that aggregation represents a common testbed for fundamental processes such as for instance the dynamical arrest of soft materials or glasses [3]. In addition, aggregating colloidal particles with tuned interaction potential are very often remarkably good in mimicking other soft materials of industrial interest such as food (yoghurt, cheese, ...), paint, and in general all gel-like materials [4,5]. Traditionally, the technique widely used for studying colloidal aggregation is light scattering, which captures the relevant length and time scales of the entire process [6]. Much work has been done with static and dynamic light scattering, especially in the low-angle regime, where the information about the size of the

[a] e-mail: roberto.cerbino@unimi.it

largest clusters can be obtained. Low angle scattering is not an easy method because of the large amount of stray light unavoidably present at small scattering angles. Dealing with stray light requires using high quality optical elements and sample cells, extremely clean samples and good background subtraction procedures. Alternatively, colloidal aggregates can be studied with confocal microscopy, but this technique is generally limited to particles large enough to be optically resolved [7].

This limitation has been overcome with the advent of a novel technique that uses a commercial bright-field microscope as a low-angle scattering instrument, despite the limited coherence of the microscope light source. The method, named Differential Dynamic Microscopy (DDM) is based on Fourier analysis of microscope movies and it was used profitably with diffusing colloidal particles of various sizes, in particular with sub-diffraction ones [8,9], and also with bacteria [10]. The advantage of DDM relies on its extreme simplicity and on the fact that it does not need much more than a microscope, a video camera and a personal computer for performing the data analysis.

In this work we take advantage of these features and use DDM for the characterization of a colloidal aggregation process induced by adding salt to a dilute colloidal suspension of 73 nm (diameter) particles. The kinetics of the aggregation is monitored during a time period of few hours and, at various times during the aggregation process, the radius of the aggregates is extracted from the study of their dynamics. We find that the aggregate radius grows as a power law of time, with an exponent compatible with a diffusion-limited cluster aggregation process. Our results show the potential of DDM for the time resolved study of aggregation and other self-organization processes in colloids.

2 Fundamentals of colloidal aggregation

Water-based colloidal suspensions are very often stabilized against aggregation by the presence of charges on the surface of the colloidal particles [2]. The overall interaction potential between two colloidal particles can thus be considered as the sum of two opposing terms: a short-range Van der Waals attraction and a long-range screened Coulomb repulsion. In normal conditions the long ranged nature of the repulsion prevents the particles from getting so close to feel the Van der Waals attraction. This stabilization can be reduced by adding a suitable amount of electrolyte to the solution, which screens the particle charge. If a sufficient amount of electrolyte is added, the repulsive term becomes too small to oppose aggregation and when two particles are brought to contact by Brownian motion they can irreversibly stick together and start forming aggregates (or clusters). In a colloidal suspension with a number density of the colloids c_0 (cm^{-3}) the typical timescale that governs the diffusive encounters of particles is given by

$$\tau_{enc} = \frac{3\eta}{4k_B T}\frac{1}{c_0} \tag{1}$$

where T is the absolute temperature of the system, k_B is the Boltzmann constant, and η the viscosity. Therefore, in general larger colloids concentrations favor quick aggregation processes and, interestingly, τ_{enc} does not depend on the particle radius R_0.

When the activation barrier is so low that every particle encounter leads to irreversible sticking the aggregation process is termed a diffusion limited aggregation or, under the more realistic assumption that also cluster can aggregate, a diffusion-limited cluster aggregation (DLCA). On the contrary, in the presence of a small but non negligible activation barrier, two particles or clusters may need to meet many times before sticking to each other and the process is said to be a reaction-limited cluster aggregation (RLCA). In both cases the structure of the aggregates is *fractal*

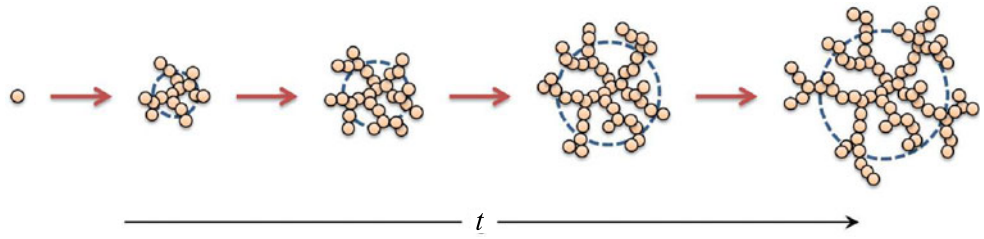

Fig. 1. Pictorial description of the growth of a fractal colloidal aggregate. The gyration radius R_G of the aggregate increases with time. For DLCA, $R_G \sim t^{1/d_f}$, whereas for RLCA the growth is exponential.

i.e. invariant to a change of scale. The mass M of a fractal object scales with the object radius R to the power d_f, which is termed (mass) fractal dimension and satisfies $1 \leq d_f \leq 3$. In general the density ρ scales as $\rho(R) \propto R^{d_f-3}$ and smaller fractal dimensions correspond to empty objects, while a space filling object such a sphere has $d_f = 3$.

It is known that most of the features of fractal aggregates do not depend on the microscopic and/or chemical details of the colloid system and that fractal aggregation is a universal process [11]. DLCA aggregates have a fractal dimension of 1.75–1.8, independent on the fact that the colloidal particles are made of gold, polystyrene or silica. In a similar way, RLCA leads to more compact objects having $d_f \simeq 2.1$–2.2.

The aggregation regime implies also different laws for the growth of the aggregates with time t. If we denote with R_G the gyration radius of the aggregate, it is known that for DLCA $R_G \sim t^{1/d_f}$ (the mass grows linearly with time), whereas for RLCA the growth is exponential. This growth is not indefinite and aggregation stops when the growing clusters touch each other. In the simplest model, where all the clusters are considered to be equal in size, this occurs when $R_G = R_G^{arr} \sim R_0 \phi_0^{\frac{1}{d_f-3}}$, where ϕ_0 is the initial colloid volume fraction. In this situation the aggregation leads to gelation, the gel being a space-spanning assembly of fractal aggregates of size R_G^{arr}, inversely dependent on the initial particle concentration. At every stage during the growth process, the cluster mass distribution $N(M)$ is dramatically different for DLCA and RLCA. For DLCA $N(M)$ is slightly peaked around the average cluster mass $\tilde{M}$, and falls exponentially for large M. For RLCA $N(M)$ has a power law behavior and exhibits a similar exponential decay beyond the peak. Intermediate aggregation modes between DLCA and RLCA have also been reported [12].

2.1 Light scattering from colloidal aggregates

In the past, the structural properties of the aggregates have been probed by means of light scattering. In static light scattering experiments, the time-averaged scattered intensity $I(q)$ is measured as a function of the scattering wave vector $q = 2nk_0 \sin(\theta/2)$ where θ is the scattering angle, n is the refractive index of the dispersion medium, and k_0 is the vacuum wavevector of the incident light. For $qR_0 \ll 1$, $I(q)$ is well approximated by the Fisher-Burford expression

$$I(q) = \frac{I(0)}{\left[1 + \frac{2(qR_g)^2}{3d_f}\right]^{\frac{d_f}{2}}}. \tag{2}$$

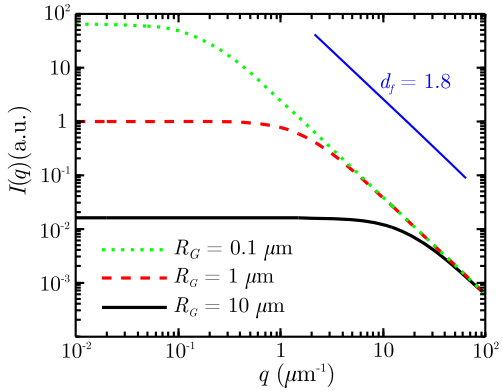

Fig. 2. The intensity $I(q)$ of the light scattered by a colloidal aggregate growing in the DLCA regime. The curves are obtained by using Eq. (2) for three values of the gyration radius: $R_G = 0.1, 10, 100\,\mu$m.

$I(q)$ exhibits a power law behavior $I(q) \sim q^{-d_f}$ for $qR_G \gg 1$ and plateaus to the value $I(0)$ for $qR_G \ll 1$. $I(0)$ is proportional to the product of the (weight average) mass cluster $M_W \sim R_G^{d_f}$ with the monomer concentration c_0. The behavior of $I(q)$ is reported in Fig. 2 for three values of R_G for a DLCA process.

As far as the dynamics is concerned, dynamic light scattering (DLS) has been used to characterize the temporal fluctuation of the scattering intensity resulting from the aggregate's motion. DLS can access the so called intermediate scattering function $f(q,t)$ via measurements of the intensity autocorrelation function [13]. It is known that for a dilute collection of Brownian particles $f(q,t) = \exp(-t/\tau_0(q))$, where $\tau_0(q) = (D_0 q^2)^{-1}$ and

$$D_0 = \frac{k_B T}{6\pi\eta R_0} \tag{3}$$

is the mass diffusion coefficient of the particles. For a system made of particle clusters the situation is more complicated and $f(q,t)$ becomes in general non-exponential [11]. However, a first cumulant analysis can be performed, which gives the short-time dynamics of the cluster and an effective diffusion coefficient $D_{\mathit{eff}}(q)$ that probes both translational diffusion of the clusters and their internal motions. For $qR_G \ll 1$ only translational diffusion contributes and one has $D_{\mathit{eff}}(q) = k_B T/(6\pi\eta R_H)$, where R_H is the average hydrodynamic radius of the cluster, which in this case is given by $R_H \simeq R_G$ [14]. For larger wavevectors, DLS probes internal motions of the clusters such as rotational diffusion and internal vibrations. A universal behavior is found for $D_{\mathit{eff}}(q)/D_{\mathit{eff}}(0)$, which increases from 1 to a value of the order of 2–3 for DLCA and 7–8 for RLCA [11].

3 Differential dynamic microscopy (DDM)

DDM belongs to the class of near field (or deep-Fresnel) scattering techniques [15–18]. Under quite general hypotheses – mainly that the sample does not scatter light multiply – scattering information is obtained by analyzing movies of images acquired close to the sample, rather than in the sample far-field. A thorough description of DDM can be found in Refs. [8,9]. The intensity of the microscope images is given by

$$I(x,y,t) = |E_0(x,y) + E_s(x,y,t)|^2 \simeq I_0(x,y) + 2\Re[E_0^*(x,y)E_s(x,y,t)] \tag{4}$$

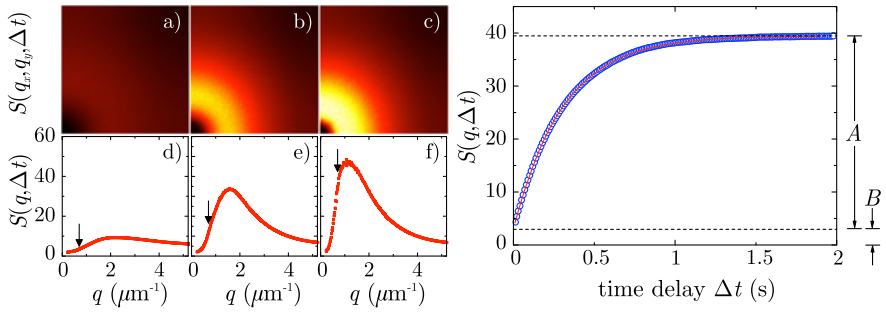

Fig. 3. (Left) The two-dimensional image structure function $S(q_x, q_y, \Delta t)$ (a,b,c) and the corresponding azimuthal averages $S(q, \Delta t)$ (d,e,f) for different values of the time delay Δt for a colloidal suspension of non-aggregating 73 nm particles. $\Delta t = 0.01$ s for (a) and (d). $\Delta t = 0.1$ s for (b) and (e). $\Delta t = 1$ s for (c) and (f). (Right) The azimuthal average $S(q, \Delta t)$ as a function of the time delay Δt for $q = 0.7\,\mu\text{m}^{-1}$, indicated with a vertical arrow in d), e), and f). A and B are the fitting parameters in Eq. (7).

where we have assumed that the transmitted intensity $I_0 = E_0^* E_0$ dominates over the scattering intensity $I_s = E_s^* E_s$ (heterodyne condition). Equation (4) shows a fundamental feature of deep Fresnel experiments i.e. the measured intensity $I(x, y, t)$ provides direct access to the real part of the scattering field $E_s(x, y, t)$. Another important feature, which will be used here, is that by subtracting images acquired at different times t and $t + \Delta t$, I_0 disappears from the problem and one obtains, for the difference signal $d(x, y, t_0, \Delta t) = I(x, y, t_0 + \Delta t) - I(x, y, t_0)$ the expression

$$d(x, y, t_0, \Delta t) = 2\Re\{E_0^*(x, y)[E_s(x, y, t_0 + \Delta t) - E_s(x, y, t_0)]\}. \tag{5}$$

In a typical experiment, a sequence of N images (usually of the order of a few thousand) is acquired at a fixed frame rate. For each time delay Δt of interest, $d(x, y, t_0, \Delta t)$ is calculated. The spatial Fourier power spectrum of d is computed and, in the presence of stationary or quasi-stationary statistical processes, an average over power spectra with the same Δt but different t_0 is obtained, which increases the statistical accuracy of the data. The final result is the so called *image structure function*

$$S(q_x, q_y, \Delta t) = \left\langle \left| \int dq_x dq_y \, \exp[-\imath(xq_x + yq_y)] \, d(x, y, t_0, \Delta t) \right|^2 \right\rangle_{t_0}. \tag{6}$$

In many cases of interest the image structure function bears a circular symmetry, as in Fig. 3(a–c), where we represent the top-right quarter of $S(q_x, q_y, \Delta t)$ for the dilute colloidal suspension of the nanoparticles used in this work for three different values of Δt. Given the circular symmetry, the azimuthal average for $q = \sqrt{q_x^2 + q_y^2}$ can be performed. Azimuthal averages for the data in Fig. 3(a–c) are presented in Fig. 3(d–f). It is visible that the signal increases as a function of Δt. This increase can be studied for every q by plotting $S(q, \Delta t)$ as a function of Δt. For example, data points such as those presented in the right panel of Fig. 3 are the result of such an analysis for $q = 0.7\,\mu\text{m}^{-1}$, marked with a vertical arrow in Fig. 3(d-f). The trend of the experimental data points can be fitted with a theoretical expression that reads

$$S(q, \Delta t) = A(q)[1 - f(q, \Delta t)] + B(q) \tag{7}$$

where $B(q)$ is a background term that accounts for the noise of the detection chain; $A(q) = T(q)I(q)$, where $I(q)$ is the intensity scattered by the sample and $T(q)$ is a

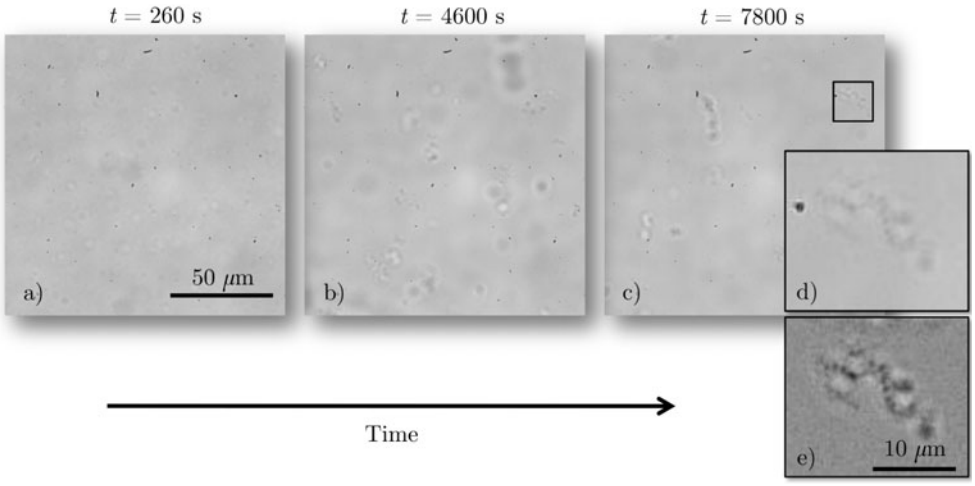

Fig. 4. Example of microscope images acquired at different times during the process of aggregation of subdiffraction particles (diameter 73 nm): a) $t = 260\,\mathrm{s}$, b) $t = 4600\,\mathrm{s}$, c) $t = 7800\,\mathrm{s}$. Figure d) is an enlargement of a portion of c), showing one of the aggregates present in the colloid. e) is the result of the subtraction between an image taken at $t = 7800\,\mathrm{s}$ and one at a time 60 seconds later when the aggregate has moved out of the region of interest. In each image, the individual nanoparticles are not visibile because of their small size.

transfer function that depends on the microscope [9]. We stress that the intermediate scattering function $f(q, \Delta t)$ is the same that would be measured in scattering experiments with the same sample.

The procedure just outlined for the data analysis is based on the fact that the spatial Fourier transform operation, which is a natural consequence of light propagation in far field experiments, is performed in DDM directly on the real space images. However, before Fourier transforming, the image subtraction procedure removes any time-independent background contribution that would show up as a non additive contribution in the far-field scattering pattern. This image subtraction procedure is one of the strengths of DDM, and together with the extreme simplicity of its implementation guarantees a relatively immediate access to low-angle scattering information at low cost. The effect of using a microscope is all contained in the transfer function $T(q)$, which mirrors the effect of the bandwidth and of the numerical aperture of the light source, the numerical aperture of the microscope objective, and the finite thickness of the sample [9]. It is worth mentioning that, when all these effects are not present, $T(q)$ coincides with the known results for other near field scattering techniques [15] such as shadowgraphy [16] and heterodyne near field scattering [17,18].

4 The experiment

In this section we describe the steps needed for preparing a DDM experiment with aggregating colloidal particles and the protocols for the image acquisition and treatment.

A DDM experiment is simple to carry out. A sample is placed in the object plane of a standard laboratory microscope. The aperture of the condenser lens is kept at its minimum to guarantee the largest degree of coherence of the illuminating light [9].

A high speed camera is positioned in the image plane, and interfaced to a personal computer with image acquiring software.

To study the aggregation process, the colloid was prepared and let aggregate in a 10 mm optical path cuvette. The samples consisted of 73 nm (Duke Scientific, Part No. 3070A) particles diluted with deionized distilled water to an initial volume fraction equal to 1.38×10^{-5}. The aggregation kinetics was monitored by using a commercial spectrophotometer (Ocean Optics HR2000CG-UV-NIR) and an halogen lamp (Ocean Optics DH 2000) coupled with two fiber optics collimators used for shining and collecting the light transmitted by the sample. The use of an optical fiber collimator (which acts as a spatial filter) for the light detection ensures that, late in the aggregation process, the light scattered in the forward direction by large aggregates does not re-enter the collection optics [19] and, therefore, does not affect the measurement of the transmitted power. To trigger the aggregation, a small volume of a properly concentrated $MgCl_2$ solution was added to the cuvette, via a pipette to reach a final particles concentration equal to $c_0 = 5.60 \times 10^{10}\,\mathrm{cm}^{-3}$ (volume fraction 1.14×10^{-5}). The final salt concentration in solution (8 mM) determined the rate at which the particles aggregated, and we could monitor this through changes in turbidity. After an appreciable change in turbidity, a small amount of sample was soaked from the cuvette into a capillary tube with rectangular cross-section (0.1(height) × 2.0 (width) mm)). Care was exerted to avoid an excessive shearing of the sample during the loading procedure. The capillary was then sealed with vacuum grease and fixed on the microscope (Nikon Eclipse Ti-U, inverted) stage. The image was formed on the sensor plane of the camera by means of a 40X objective (NA = 0.55). Eight acquisitions were taken during the aggregation process, along with a measure of the monomer prior to adding salt.

For each acquisition, a sequence of $N = 8000$ images was recorded with a digital video camera (Allied Vision Prosilica GX1050, Kodak KAI-01050 CCD sensor, 1024 × 1024 pixels, pixel size = 5.5 μm, binning 2 × 2, exposure time 1.5 ms). Due to the initially fast diffusion and dynamics, the frame rate was set at 100 frames per second (fps), near the limit of the camera speed. As the aggregation process continued, the dynamics slowed, thus we took images at both 100 fps and 10 fps in order to capture an appreciable variation in position of the aggregates. In principle, the growth of the aggregates during the acquisition of each image dataset could affect the results of our analysis. As a simple check that this was not the case, we split each dataset in two halves and the results of the DDM analysis on each half were compared. For all the datasets reported here no appreciable differences were found and, as an additional precaution, each dataset was labeled by using the time delay Δt corresponding to the 4000th frame of each acquisition.

5 Results

The images from each acquisition were saved in binary format to a personal computer, using a custom National Instruments LabVIEW program. Post processing was done with custom MATLAB and LabVIEW software, by implementing algorithms based on the techniques described in Sect. 3. A detailed overview of the data analysis is reported here. Shown in Fig. 5(a) is the plot of $S(q, \Delta t)$ as a function of q for thirteen different time delays (Δt) starting from 0.01 s (lowest curve plotted) up to 40 s (higher curve). The curve $\Delta t = 40$ s is representative of all the curves that were obtained for longer Δt. Note that the delay times reported in Fig. 5(a) are not evenly spaced, showing that the increase of $S(q, \Delta t)$ is more pronounced for small Δt and reaches a stationary regime for Δt larger than 20 s. The same behaviour is confirmed in Fig. 5(b). Here $S(q, \Delta t)$ is plotted as a function of Δt for four chosen values of q,

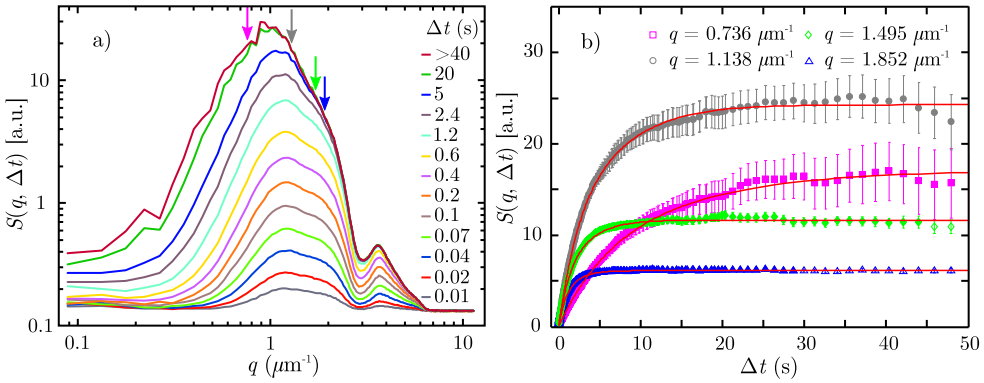

Fig. 5. a) Plot of $S(q, \Delta t)$ as a function of q for thirteen different time delays (Δt) starting from 0.01 s (lowest curve plotted) up to 40 s (highest curve).The four arrows are indicative of the q values chosen for the plots in figure b). b) Plot of the experimental data of $S(q, \Delta t)$ for four representative q values and of the corresponding power law fit. The data correspond to the acquisition at $t = 1760$ s.

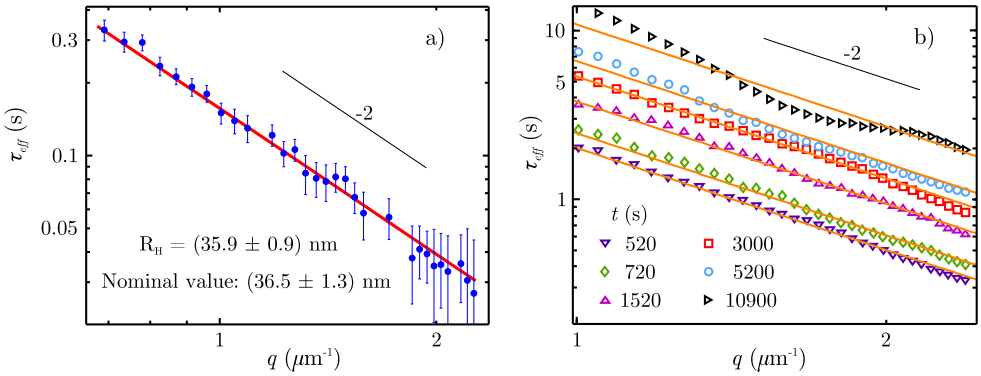

Fig. 6. Plot of $\tau_{eff} = 1/(D_{eff} q^2)$ as a function of q for the unaggregated monomers (a) and for acquisitions taken at six different instances in the aggregation process (b). Also shown are the power law fit obtained fixing the exponent at -2.

namely $q = 0.736\,\mu\text{m}^{-1}$, $q = 1.138\,\mu\text{m}^{-1}$, $q = 1.495\,\mu\text{m}^{-1}$ and $q = 1.852\,\mu\text{m}^{-1}$. For large Δt, $S(q, \Delta t)$ plateaus to a constant value, as expected from theory. Experimental data have been fitted using the cumulant method (see [20] for a relatively recent review of the method), which allowed us to recover an effective decay time τ_{eff} and its level of polydispersity (data not shown). Error bars were estimated by taking into account the number n of effective independent measurements taken for all the power spectra with the same time delay (Δt) during the entire measuring time T_{meas} ($n \sim [T_{meas} - \Delta t]/\tau_{eff}$). This procedure leads to error bars that become larger with increasing Δt correlation times, as shown in Fig. 5(b).

Figure 6 investigates the behaviour of $\tau_{eff} = 1/(D_{eff} q^2)$ for different q, derived from the fitting procedure of the $S(q, \Delta t)$ curves as function of Δt [Fig. 5(b)], for each different instance in the aggregation process (right panel) as well as for the monomer prior to aggregation (left panel). Data fitting has been performed keeping the slope at a fixed value of -2. The measurement performed before aggregation provided the estimate $R_H = (35.9 \pm 0.9)$ nm, in good agreement with the nominal

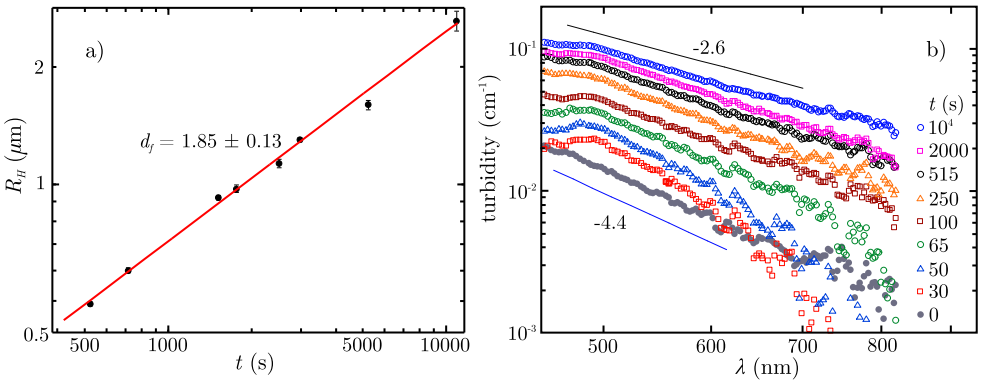

Fig. 7. a) Plot of the Hydrodynamic radius R_H of the aggregates as function of time. Experimental data and power law fit are shown. The fractal dimension obtained from the slope of the line is $d_f = 1.85 \pm 0.13$. b) Plot of the turbidity at different aggregation times. At $t = 0\,\mathrm{s}$ the line shows a $\lambda^{-4.4}$ behaviour. As the aggregation process develops $\lambda^{-2.6}$ behaviour is reached.

value $R_H = (36.5 \pm 1.3)\,\mathrm{nm}$ from the producer. For the aggregates, for small times t the power law fit is in good accordance with the experimental data. For larger times, the agreement between experimental and fitted data becomes less representative, as a consequence of the expected effects of clusters rotation and vibration. However, the quality of our data points did not allow a systematic study of this deviation and of the detailed behavior of $D_{eff}(q)$. The limiting factor was that for increasing cluster sizes, the number of clusters within the region of interest decreased too much, as visible in Fig. 4. This limitation could be overcome in future experiments by reducing the magnification of the optical system.

To conclude the data analysis, shown in Fig. 7(a) is the effective hydrodynamic radius of the aggregates as a function of time, recovered by means of Eq. (3). The data were best fitted with a power law implying that a diffusion limited aggregation (DLCA) took place. The fractal dimension was found to be $d_f = 1.85 \pm 0.13$, in accordance with a DLCA process.

Figure 7(b) is a plot of the data acquired monitoring the evolution of sample 1 with the fiber optic spectrometer. The data show that the behavior of the turbidity as a function of the wavelength λ goes from the pure Rayleigh regime (turbidity $\sim\lambda^{-4.4}$) at $t = 0\,\mathrm{s}$, to $\sim\lambda^{-2.6}$ in the presence of large fractal aggregates ($t = 10000\,\mathrm{s}$).

We can compare the results obtained by using the DDM technique with the ones deriving from the turbidity measurement. As known [21] at the late stage of a fractal colloidal aggregation process (when $R_g \gg \lambda$), the turbidity is expected to scale as $\sim\lambda^{-(4-d_f)}$. However, due to the wavelength dispersion of the refraction indexes of both polystyrene and water [19] the exponent -4 expected from Rayleigh scattering is modified into an effective exponent of -4.4. Thus, from the slope measured for the latest time, we recover a value of $d_f = 4.4 - 2.6 = 1.8$ which is in excellent agreement with the fractal dimension obtained from the DDM technique.

6 Conclusions

In this study, we have shown the viability of DDM in studying the dynamic aggregation processes in colloidal systems. Using simply a standard laboratory microscope

equipped with a high speed camera, we were able to estimate the hydrodynamic radius of aggregates as a function of time up to sizes many μm. Control of the aggregation process was achieved through altering the concentration of salt and nanoparticles. The samples used here showed a power law growth of the gyration radius from which a fractal dimension has been extracted. The DDM results are compatible with a diffusion limited aggregation process, as independently confirmed by spectral measurements of the light transmitted by the aggregating sample.

The experiment has been performed in the context of STELLA, the School for Training in Experiments with Lasers and Laser Applications, held at the Insubria University in Como from June 20 to July 8, 2011 (see `http://www.stella-school.eu`). The Authors wish to acknowledge CARIPLO, UNIVERCOMO and Banca del Monte di Lombardia Foundations for having financed the project. The Authors like also to acknowledge the STELLA-school students O. Broekmans, M. Bina, M. Turconi for their contribution in developing the experimental apparatus, in performing the measurements and in implementing the analysis software, and Prof. P. Di Trapani for fund raising and project coordination. The Authors acknowledge Nikon Corporation, in the person of Dr. Martella, for the loan of the microscope.

References

1. W.B. Russel, D.A. Saville, W. Schowalter, *Colloidal Dispersions* (Cambridge University Press, Cambridge, 1992)
2. R.J. Hunter, *Foundations of Colloid Science* (Oxford University Press, Oxford, 2001)
3. V. Trappe, P. Sandkühler, Curr. Op. Coll. Int. Science **8**, 494 (2004)
4. R. Mezzenga, P. Schurtenberger, A. Burbidge, M. Michel, Nature Mater. **4**, 729 (2005)
5. P. Zakharov, F. Scheffold, Soft Materials **8**, 102 (2010)
6. C.M. Sorensen, Aerosol Sci. Technol. **35**, 648 (2001)
7. V. Prasad, D. Semwogerere, E.R. Weeks, J. Phys.: Cond. Mat. **19**, 113102 (2007)
8. R. Cerbino, V. Trappe, Phys. Rev. Lett. **100**, 188102 (2008)
9. F. Giavazzi, D. Brogioli, V. Trappe, T. Bellini, R. Cerbino, Phys. Rev. E **80**, 031403 (2009)
10. L.G. Wilson, V.A. Martinez, J. Schwarz-Linek, J. Tailleur, G. Bryant, P.N. Pusey, W.C.K. Poon, Phys. Rev. Lett. **106**, 018101 (2011)
11. M.Y. Lin, H.M. Lindsay, D.A. Weitz, R.C. Ball, R. Klein, P. Meakin, Nature **339**, 360 (1989)
12. D. Asnaghi, M. Carpineti, M. Giglio, M. Sozzi, Phys. Rev. A **45**, 1018 (1992)
13. B.J. Berne, R. Pecora, *Dynamic Light Scattering: With Applications to Chemistry, Biology, and Physics* (Dover, New York, 2000)
14. P. Wiltzius, Phys. Rev. Lett. **58**, 710 (1987)
15. R. Cerbino, A. Vailati, Curr. Op. Coll. Int. Science **14**, 416 (2009)
16. F. Croccolo, D. Brogioli, A. Vailati, M. Giglio, D.S. Cannell, Ann. NY Acad. Sci. **1077**, 365 (2006)
17. F. Ferri, D. Magatti, D. Pescini, M.A.C. Potenza, M. Giglio, Phys. Rev. E **70**, 041405 (2004)
18. D. Magatti, M. Alaimo, M.A.C. Potenza, F. Ferri, Appl. Phys. Lett. **92**, 241101-1/3 (2008)
19. F. Ferri, A. Bassini, E. Paganini, Appl. Opt. **36**, 885 (1997)
20. B.J. Frisken, Appl. Opt. **40**, 4087 (2001)
21. D.S. Horne, Faraday Discuss. Chem. Soc. **83**, 259 (1987)